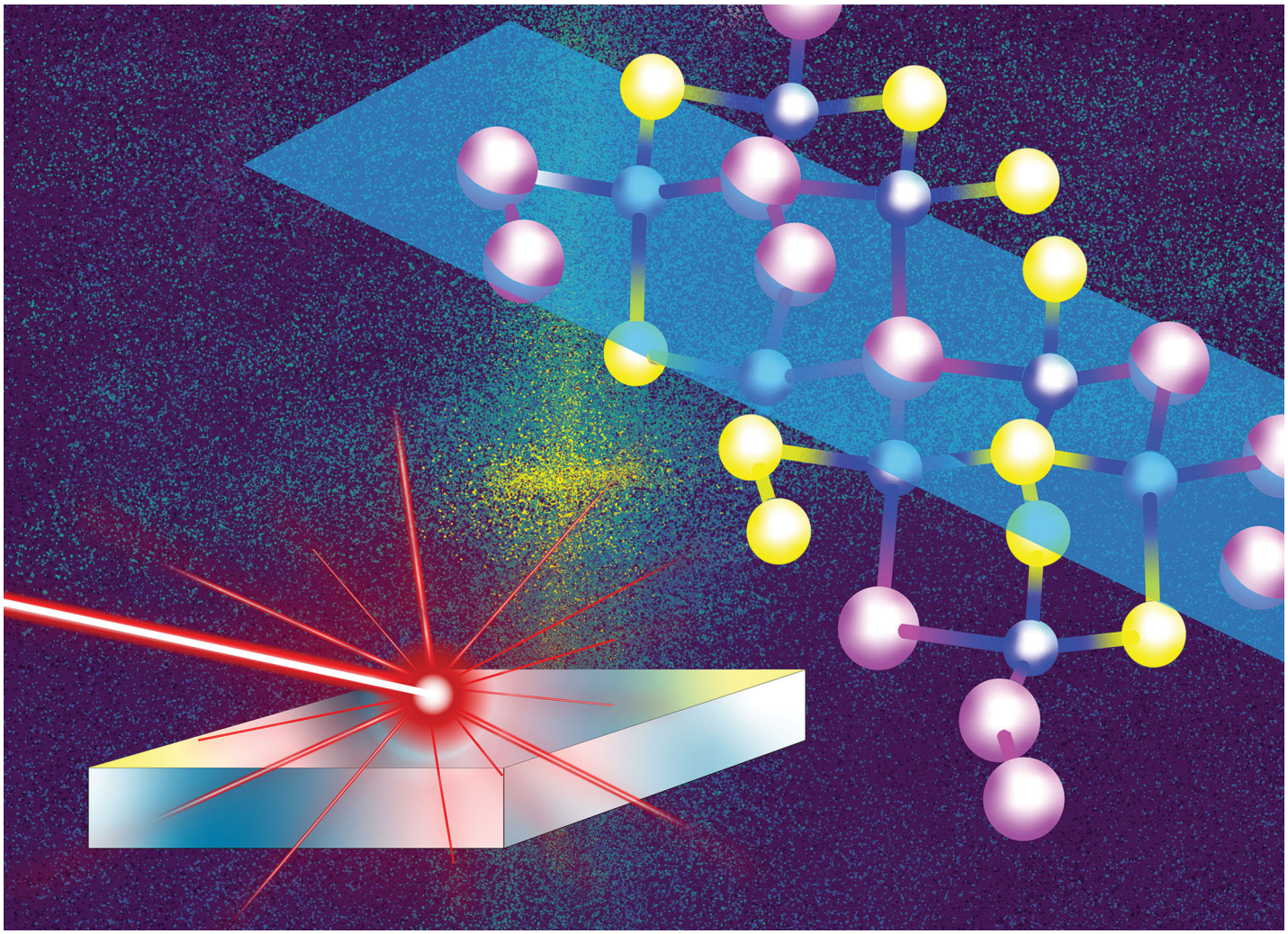

Showcasing collaborative research from the Colorado School of Mines, National Renewable Energy Lab, and SLAC National Accelerator Laboratory

Using resonant energy X-ray diffraction to extract chemical order parameters in ternary semiconductors

Resonant energy X-ray diffraction was used to quantify the degree of cation site disorder in $ZnGeP_2$ thin films and reveal a trend of lower absorption onset energy with increased disorder. These results highlight the potential for tuning properties in ternary materials through site disorder.

As featured in:

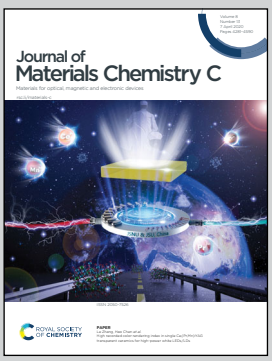

See Adele C. Tamboli *et al.*, *J. Mater. Chem. C*, 2020, **8**, 4350.

ROYAL SOCIETY OF CHEMISTRY

rsc.li/materials-c

Registered charity number: 207890

Journal of Materials Chemistry C

ROYAL SOCIETY OF CHEMISTRY

PAPER

View Article Online
View Journal | View Issue

Check for updates

Cite this: J. Mater. Chem. C, 2020, 8, 4350

Using resonant energy X-ray diffraction to extract chemical order parameters in ternary semiconductors†

Rekha R. Schnepf, [ab] Ben L. Levy-Wendt, [cd] M. Brooks Tellekamp, [a] Brenden R. Ortiz, [b] Celeste L. Melamed, [ab] Laura T. Schelhas, [c] Kevin H. Stone, [c] Michael F. Toney, [c] Eric S. Toberer [ab] and Adele C. Tamboli *[ab]

II–IV–V_2 materials, ternary analogs to III–V materials, are emerging for their potential applications in devices such as LEDs and solar cells. Controlling cation ordering in II–IV–V_2 materials offers the potential to tune properties at nearly fixed compositions and lattice parameters. While tuning properties at a fixed lattice constant through ordering has the potential to be a powerful tool used in device fabrication, cation ordering also creates challenges with characterization and quantification of ordering. In this work, we investigate two different methods to quantify cation ordering in $ZnGeP_2$ thin films: a stretching parameter calculated from lattice constants $\left(\frac{c}{a}\right)$, and an order parameter determined from the cation site occupancies (S). We use high resolution X-ray diffraction (HRXRD) to determine $\frac{c}{a}$ and resonant energy X-ray diffraction (REXD) to extract S. REXD is critical to distinguish between elements with similar Z-number (*e.g.* Zn and Ge). We found that samples with a $\frac{c}{a}$ corresponding to the ordered chalcopyrite structure had only partially ordered S values. The optical absorption onset for these films occurred at lower energy than expected for fully ordered $ZnGeP_2$, indicating that S is a more accurate descriptor of cation order than the stretching parameter. Since disorder is complex and can occur on many length scales, metrics for quantifying disorder should be chosen that most accurately reflect the physical properties of interest.

Received 7th December 2019,
Accepted 3rd March 2020

DOI: 10.1039/c9tc06699c

rsc.li/materials-c

Published on 12 March 2020. Downloaded by Northwestern University on 9/29/2020 9:16:38 PM.

1 Introduction

The ternary and multinary analogs of successful binary materials are increasingly being studied for their potential integration in optoelectronic devices. For example, Cu_2ZnSnS_4 (CZTS) and $Cu_2ZnSnSe_4$ (CZTSe), derived from the II–VI material family, have been well studied for photovoltaic applications.[1] Similarly, II–IV–V_2's, the ternary analogs to III–V's, are emerging for their potential optoelectronic applications. The increased complexity in II–IV–V_2's enables tunable properties at nearly fixed lattice parameters through cation site ordering.[2] This added tunability of properties in conjunction with similar lattice constants to III–V's makes these materials exciting for integration into existing technologies. However, as has been shown with CZTS, the detection and understanding of cation site ordering is not trivial.

There has already been extensive work conducted on understanding ordering in CZTS, and there are several lessons that can be learned. It has been known since the 1970s that CZTS and related $A_2^IB^{II}C^{IV}X_4^{VI}$ compounds can exist in both the kesterite (space group $I\bar{4}$) and stannite (space group $I\bar{4}2m$) structures.[3] It is very difficult to tell these two structures apart since they have very similar lattice constants and only differ in the occupancy of Cu and Zn sites.[4–6] The similarities in the two structures and the fact that Cu and Zn have similar Z number results in an almost indistinguishable conventional XRD pattern.[4,7] However, distinguishing between the two structures was vital to device integration since the stannite structure is predicted to have a smaller band gap than the kesterite structure.[7] First principles calculations in 2009 predicted that $A_2^IB^{II}C^{IV}X_4^{VI}$ compounds are more stable in the kesterite structure and that experimental studies showing the presence of stannite were actually due to partial disorder of the Cu and Zn in the (001) layer of the kesterite phase.[5,8]

[a] National Renewable Energy Laboratory, Golden, CO, USA.
E-mail: adele.tamboli@nrel.gov; Fax: +1-303-384-7600; Tel: +1-303-384-7223
[b] Department of Physics, Colorado School of Mines, Golden, Colorado, USA
[c] SLAC National Accelerator Laboratory, Menlo Park, California, USA
[d] Department of Mechanical Engineering, Stanford University, Stanford, CA, USA

† Electronic supplementary information (ESI) available. See DOI: 10.1039/c9tc06699c

This journal is © The Royal Society of Chemistry 2020

Published on 12 March 2020. Downloaded by Northwestern University on 9/29/2020 9:16:38 PM.

This was hard to verify experimentally since standard X-ray diffraction is not able to differentiate between elements of similar *Z*-number. In a 2011 neutron diffraction study, Schorr confirmed that CZTS and CZTSe crystallize in the kesterite structure and identified intrinsic antisite defects Cu_{Zn} and Zn_{Cu} that result in partial disorder of the (001) layer.[9] In this case, neutron diffraction was key to understanding disorder in bulk CZTS and CZTSe; however, neutron diffraction is not well suited to thin films, due to the smaller scattering cross section, so another approach is necessary for quantifying cation ordering.[10]

A standard approach to quantifying long range order in ternary materials is to determine a long range order parameter based on lattice site occupancies. For example, the Bragg–Williams long range order parameter, S, is defined as: $S = r_\alpha + r_\beta - 1$, where r_α and r_β are the fraction of α and β sites occupied by the correct atom.[11] In a perfectly ordered and stoichiometric material, $S = 1$, and in a fully disordered material, $S = 0$. In a 2017 study on $ZnSnP_2$, Nakatsuka and Nose used X-ray diffraction (XRD) data to evaluate the Bragg–Williams order parameter in $ZnSnP_2$ samples using two different methods.[12] In the first method, they took the peak area ratio of a superlattice to fundamental reflection to determine the long range order parameter. This method takes advantage of the fact that the transition to the lower symmetry ordered phase results in the emergence of superlattice reflections. In the second method, they solved for the long range order parameter using cation site occupancies from Rietveld refinement. These methods yielded nearly matching results and work well for $ZnSnP_2$ because Zn and Sn have sufficiently different atomic scattering factors. However, for elements with similar atomic number (*e.g.* Cu, Zn, and Ge), they are indistinguishable through conventional XRD methods. Additionally, because the intensity of the superlattice peaks relies on there being a difference in scattering factors between the two cations, for elements with similar *Z* number the superlattice peaks are extremely small and often below the noise level of the data.[13] Due to the challenges that arise when cations have similar *Z* number, alternative methods to quantify ordering are necessary.

In a 2017 paper on $ZnGeN_2$, Blanton *et al.* defined a stretching parameter based on lattice parameters to characterize ordering.[13] A fully disordered $ZnGeN_2$ structure exists in a wurtzite structure, while the fully ordered structure is in a wurtzite-derived orthorhombic structure where the *a* parameter has increased and the *b* parameter has decreased. This lattice distortion causes $\frac{a}{b}$ to become greater than the ideal wurtzite value of $\frac{2\sqrt{3}}{3}$. The stretching parameter can also be extended to II–IV–P_2 systems, where the disordered structure is zinc blende and the ordered structure is chalcopyrite. Due to the different bond lengths between Zn–P and Ge–P, the *c*-axis contracts when the cations aren't randomly occupying the cation sublattice, resulting in a $\frac{c}{a}$ of less than 2.[14–16] Since these lattice distortions result in a decrease in symmetry they can be detected using standard XRD through peak splitting, assuming this is sufficiently large. However, if there is a change in cation site ordering that does not result in a change in the lattice parameters then the actual cation site occupancies must be probed directly.

Resonant energy X-ray diffraction (REXD) is a technique that can serve as a solution to these challenges. It is well suited to thin films and can differentiate between atoms with similar *Z* number.[17] In a REXD experiment, XRD data is collected as a function of incident X-ray energy, while the energy is swept across the absorption edge of a constituent element in the material. The atomic scattering factor of an element is varied at its absorption edge. Since the absorption edge is unique for each element, REXD enables the selective modification of the scattering factor of an element in a sample. REXD has been successfully used to extract cation site occupancies from CZTS as well as spinel oxides.[4,17–19]

In this paper, we strive to gain a better understanding of the abilities of two methods for quantifying ordering in ternary materials: $\frac{c}{a}$ determined from Rietveld refinement on high resolution X-ray diffraction (HRXRD) data and order parameter calculated from cation site occupancies extracted from Rietveld refinement on REXD data. We grew $ZnGeP_2$ thin film samples over a range of cation compositions, from zinc poor (germanium rich) to stoichiometric, using a variety of post-growth annealing conditions. HRXRD was conducted on all the samples to calculate $\frac{c}{a}$. REXD was done on two samples, with $\frac{c}{a}$ ratios corresponding to the ordered chalcopyrite structure, to determine cation site occupancies. It was found that despite having an "ordered" $\frac{c}{a}$, these two films had only partially ordered cation site occupancies. Spectroscopic ellipsometry was used to measure the absorption coefficient of the films, which show a decreased and less steep absorption onset energy with a decrease in *S*. These results indicate that *S* is better characterizing the disorder that affects optical properties in these films than $\frac{c}{a}$.

2 Experimental methods

The samples used for REXD and HRXRD were grown on (100) Si wafers with a 4° offcut in the [111] direction using low-pressure chemical vapor deposition with a combination of hydride and elemental precursors as described by Martinez *et al.*[20] An effusion cell was used to evaporate elemental Zn onto the substrate. The Ge and P were delivered *via* 2% germane in hydrogen and 5% phosphine in hydrogen as source gases that were cracked near the substrate using tungsten hot wires. The substrate temperature was kept at 200 °C, since any efforts to increase the temperature resulted in Zn desorption. *In situ* ellipsometry was used to monitor film growth using a M-2000UI J. A. Woollam ellipsometer with a Cody–Lorentz oscillator model, and all of the films were around 300 nm thick. The low substrate temperature resulted in amorphous films, which were then annealed in quartz ampoules filled with an inert gas, either N_2 or Ar. Anneal temperatures ranged from 450 °C to 750 °C. At the end of an anneal, the films were removed from the furnace, prior to ramping down the furnace temperature.

Published on 12 March 2020. Downloaded by Northwestern University on 9/29/2020 9:16:38 PM.

A set of samples with a range of compositions was achieved through variations in composition across a single substrate, likely due to uneven heating and lack of rotation of the substrate during the original film growth. The proportion of zinc on the cation sublattice, Zn/(Zn + Ge), was determined using energy dispersive X-ray fluorescence (XRF). XRF measurements were performed using a Fischerscope X-ray XUV 773 and Fischer WinFTM software. The tool has been calibrated using Rutherford backscattering to determine an uncertainty in the XRF measurements of ±1.7%. The compositions that are reported in this paper are for the final, annealed, films.

The HRXRD measurements were performed at the Stanford Synchrotron Radiation Lightsource (SSRL) beamline 2-1 using an X-ray energy of 12 keV (λ = 1.033195 Å) and Si(111) analyzer crystal and photomultiplier tube detector. The incident angle was fixed at 3° to optimize signal from the thin films and minimize collection from the substrate. Rietveld refinements were performed on the HRXRD data to extract lattice parameters using the TOPAS 6 Academic software package. The chalcopyrite structure, $I\bar{4}2d$, was used as the base structure for the refinement. The data was fit with standard Gaussian and Lorentzian peak broadening. Cation site occupancies were given an initial guess of fully ordered and allowed to refine, but had no effect on the actual fit since non-resonant XRD cannot distinguish Zn and Ge. While these films aren't highly textured, the March–Dollase model for preferred orientation was also incorporated to account for slight texturing since these films are not perfectly randomly oriented powders. TEM images of the preferred orientation were shown in previous work.[21] The value of the *c*/*a* ratio was calculated from these refinements to compare across samples with a range of compositions and anneal conditions.

REXD measurements were performed on two samples, one annealed for one hour at 600 °C with a post-anneal composition of 51% Zn/(Zn + Ge), the other annealed for one hour at 650 °C with a post-anneal composition of 49% Zn/(Zn + Ge). Both samples had a *c*/*a* ratio close to that of the ordered structure, as shown in Fig. 1. The REXD measurements were also performed at the SSRL beamline 2-1. The incident angle was fixed at 1° and a Pilatus 100 K detector was used. Full pattern scans were conducted over a large *Q* range with incident energies at the Zinc K-edge (9659 eV), the germanium K-edge (11 103 eV) and at an off-resonant energy (10 500 eV). Data was also collected over a smaller *Q*-range at the (101) superlattice peak and (204) fundamental peak while scanning the incident beam energy across the Zn and Ge absorption edges. To scan across the Zn edge the incident beam energy ranged from 9452 eV to 9864 eV and to scan across the Ge edge it ranged from 10 897 eV to 11 309 eV.

Rietveld refinements were performed on the REXD data using a method similar to that reported by Stone *et al.*[17] First, the off-resonant full pattern was fit to extract lattice parameters, the phosphorous atomic position, the thermal parameter, and texturing. The chalcopyrite structure, $I\bar{4}2d$, was used as the base structure for the refinement. The occupancy values were then determined by simultaneously refining the full pattern scans and the scans over both the superlattice and fundamental peaks with changing energy. The Zn and Ge cation sites (Wyckoff positions 2a and 2b) were allowed to be occupied by either Zn or Ge. The total occupancy on each site was constrained such that it could not exceed one. Quadratic penalties were used to constrain the overall composition to that determined by XRF. To ensure that final occupancy values correspond to the absolute lowest *R*-value, *R*-values were collected while cycling the initial guesses for the occupancies from fully ordered to fully disordered. More detail on the results of cycling through initial occupancy values can be found in the ESI.† For the sample annealed at 650 °C, only data in the energy range of 9560 eV and 9759 eV for the Zn edge and 11 004 eV to 11 203 eV for the Ge edge were used for the refinements to increase refinement speed and due to a large amount of noise in the off-resonant scans of the (101) peak. Data above the Zn edge for the 600 °C sample was not used due to the presence of artifacts in the detector image. We believe these artifacts were caused by an error in the energy threshold settings for the detector during these measurements and only affected the data above the absorption edge. The data up to and including the edge remains sufficient for REXD analysis. Additionally, in this sample, small peaks corresponding to Zn_3P_2 were identified in

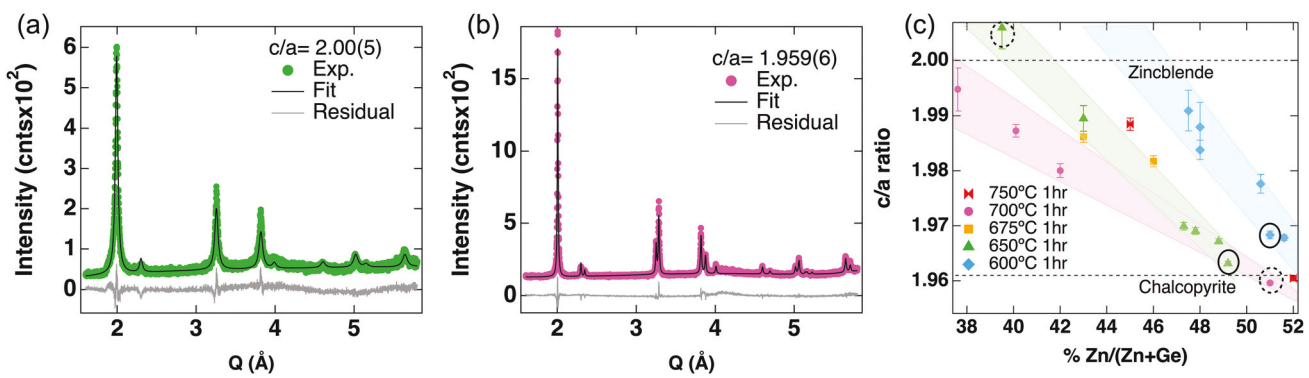

Fig. 1 Representative Rietveld refinements of HRXRD data. (a) Sample annealed at 650 °C with a composition of 39.5% Zn/(Zn + Ge) does not show peak splitting and has a *c*/*a* corresponding to the disordered structure. (b) Peak splitting is evident in a sample annealed at 700 °C with a composition of 51% Zn/(Zn + Ge) and *c*/*a* corresponding to the ordered structure. (c) The *c*/*a* ratios determined for samples with varying composition that experienced a range of anneal temperatures. The samples shown in (a) and (b) are circled with a dashed line. REXD was conducted on the films indicated by the circles with solid lines.

 This journal is © The Royal Society of Chemistry 2020

Published on 12 March 2020. Downloaded by Northwestern University on 9/29/2020 9:16:38 PM.

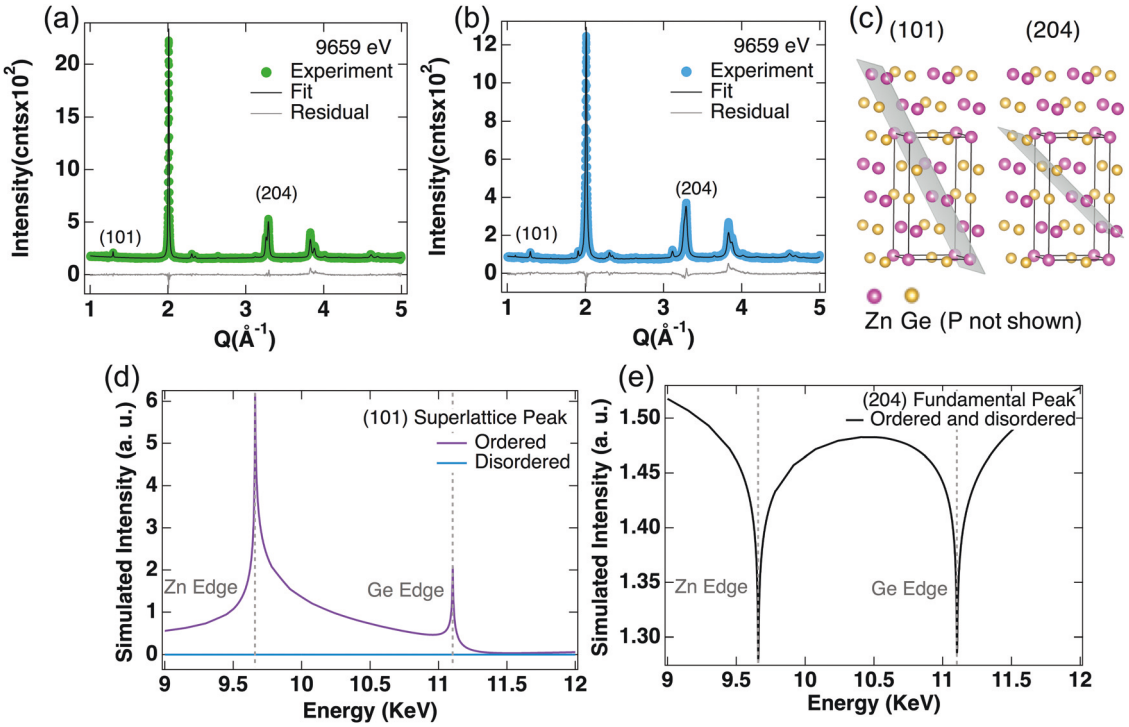

Fig. 2 Representative Rietveld refinement results of the survey scans over a large Q range at the Zn edge for the (a) sample annealed at 600 °C and (b) the sample annealed at 650 °C with the (101) and (204) peaks labelled. Differences in the intensities of fundamental peaks in (a) and (b) are likely a result of variations in texturing and crystalline quality between the two samples. (c) The (101) and (204) peaks are shown in the cation sublattice of the ordered chalcopyrite crystal structure. The (101) peak intersects cations of only one type and as a result is sensitive to ordering. The (204) peak intersects both cations and does not change intensities with ordering. (d) Simulated REXD for the (101) peak is shown at energies ranging over both the Zn and Ge edges. It can be seen that the peak has no intensity for a disordered sample and has low intensity that spikes at the absorption edges for an ordered sample. (e) Simulated REXD for the (204) illustrates that the intensity is the same for an ordered and disordered sample and the intensity dips at the absorption edges.

the full pattern scans. As a result, the Zn_3P_2 phase was included in the refinement.

REXD patterns were simulated for the (101) and (204) peak by calculating their structure factors assuming both a fully ordered and fully disordered unit cell, as shown in Fig. 2.

Ellipsometry measurements to determine absorption coefficient were conducted on the two samples that underwent REXD. The measurements were conducted using a J.A. Woollam Co. M-2000 variable angle ellipsometer at angles close to the Brewster angle of Si: 65°, 70°, 75°. The modelling was conducted in the CompleteEASE software (version 5.08) using the B-spline parameterization. The procedure was previously described by Martinez *et al.*[20]

3 Results and discussion

HRXRD was conducted on samples over a range of compositions and processing conditions, as shown in Fig. 1(c). Rietveld refinements were completed on these samples to determine their lattice parameters and calculate $\frac{c}{a}$ as a method to quantify ordering. Cation site occupancies were not extracted from this data since Zn and Ge are indistinguishable off-resonance. Fig. 1(a) shows the diffraction pattern for a sample with a $\frac{c}{a}$ of 2.00(5), suggesting a disordered structure. The diffraction pattern in Fig. 1(a) does not show peak splitting, as expected for a sample with a $\frac{c}{a} = 2.00(5)$. In Fig. 1(b), the diffraction pattern shows clear peak splitting, indicative of the lower symmetry phase, and the calculated $\frac{c}{a}$ is 1.959(7), which is close to previously reported values for the ordered chalcopyrite structure of around 1.96.[15,16,22,23] The error bars were calculated by TOPAS based on the refinement fit.

Fig. 1(c) shows a compilation of the $\frac{c}{a}$ results plotted against composition. It can be seen that samples further off stoichiometry are more zinc blende-like. As the composition becomes more Zn poor, disorder is induced since order requires near equal amounts of Zn and Ge to occupy their specific lattice sites. Fig. 1(c) also shows that samples annealed at lower temperatures have a larger $\frac{c}{a}$. This trend with anneal temperature is illustrated with the colored shading behind data points annealed at the same temperature. The samples annealed at 600 °C have a higher $\frac{c}{a}$ than the samples annealed at 650 °C and 700 °C for a given composition. The fact that lower anneal temperatures result in a more zinc blende-like structure suggests that, due to the non-equilibrium film growth, kinetics dominate the process and allow the disordered phase to exist at temperatures below the thermodynamic transition temperature. The atoms can move to crystallize at the lower temperatures, however there is still a reduced diffusion coefficient that prevents a full transition

Published on 12 March 2020. Downloaded by Northwestern University on 9/29/2020 9:16:38 PM.

to the energetically favored chalcopyrite structure. At higher anneal temperatures, atoms are better able to move into the chalcopyrite structure. While these are likely the kinetics at play, probing the average site occupancies could provide more insight on whether the fully ordered chalcopyrite structure was actually achieved.

Based on Fig. 1(c) it would seem that our samples spanned from fully disordered to fully ordered primarily by changing the film composition. REXD was conducted on the two data points circled with the solid line in Fig. 1(c), which have $\frac{c}{a}$ ratios corresponding to the fully ordered structure. If $\frac{c}{a}$ fully captured the atomic ordering of this system, one could conclude that they are both near fully ordered. However, our REXD results lead to a different conclusion.

REXD full pattern scans over a large Q range were done on both samples, one annealed at 650 °C with 49% Zn/Zn + Ge and the other annealed at 600 °C with 51% Zn/Zn + Ge, at the Zn K-edge, Ge K-edge, and off a resonant energy at 10 500 eV. The Zn edge survey scan results are shown in Fig. 2(a) and (b). The (101) superlattice peak can be seen in both scans at the Zn edge. As shown in Fig. 2(c), in a fully ordered structure the (101) planes alternate cation types. As a result, the intensity of the (101) peak will change with the degree of ordering. This is also illustrated in Fig. 2(d), which shows the simulated change in peak intensity across energy, and the disordered peak intensity is always zero. The ordered (101) peak has very low intensity off a resonant energy but the intensity spikes at the Zn and Ge absorption edges. Due to the sensitivity to ordering in the (101) peak, the intensity of this peak in our samples was studied as a function of energy. Data was also collected on the (204) peak, shown in Fig. 2(a) and (b). The (204) peak intensity does not change with the degree of ordering since each (204) plane contain both cation types equally even in the ordered structure, shown in Fig. 2(c) and (d).

REXD data was collected at the (101) and (204) peaks as a function of incident beam energy around the Zn and Ge edges. The background-subtracted Zn edge data is plotted as a heat-map in Fig. 3. The (101) and (204) peaks for the sample annealed at 650 °C are shown in Fig. 3(a) and (b), respectively. As expected, near the zinc edge, the (101) peak gains intensity while the (204) peak has a sharp drop in intensity. The data for the sample annealed at 600 °C, Fig. 3(c) and (d), shows the expected behavior up to the edge. However, after the edge the data has columnar artifacts that appear at similar Q values to the peaks, obscuring the data. As a result of these artifacts, only data up to the absorption edge was used in the Rietveld refinement for the sample annealed at 600 °C (see Fig. 4(c) and (d)).

Rietveld refinements were performed on the single energy full pattern scans and the scans over the (101) and (204) peaks while changing the incident beam energy to determine cation site occupancies and order parameter. To plot the results of the Rietveld refinements in terms of energy, as shown in figure in Fig. 4, the area under each experimental and model peak was determined at a given energy. For the (101) peaks, Simpson's rule integration was completed using Python to determine the area under the peak. The (204) peak area was fit using either a Gaussian or Voigt model, using a two peak superposition to separate the (204) peak from the (220) shoulder. The refinement results for the sample annealed at 650 °C are shown in Fig. 4(a) and (b), while the sample annealed at 600 °C is shown in Fig. 4(c) and (d). In Fig. 4, it can be seen that the models correctly capture the shape of the data. The order parameter, S,

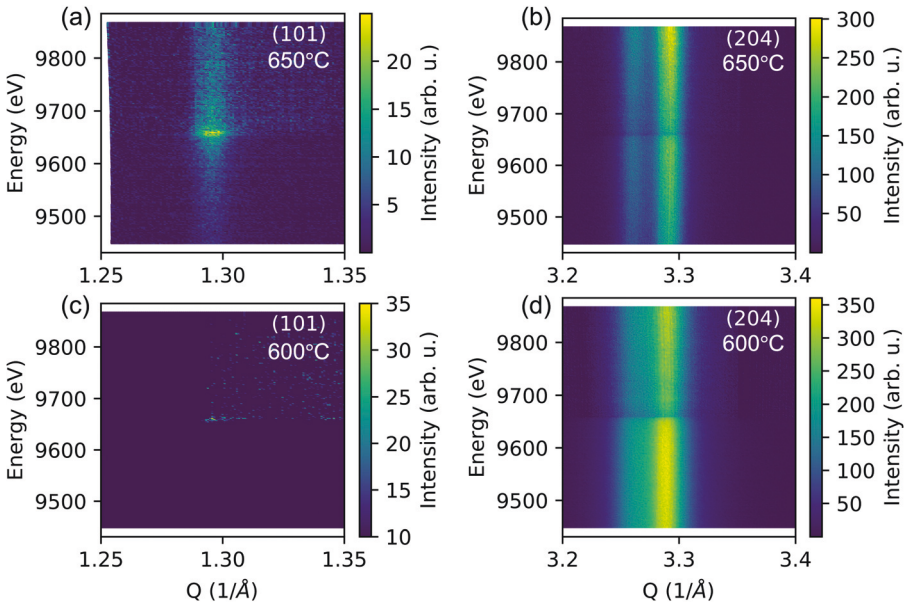

Fig. 3 Zn edge REXD data shown as a heat map. (a) and (b) show the (101) and (204) peaks across the Zn edge for the sample annealed at 650 °C, respectively. (c) and (d) show the (101) and (204) peaks across the Zn edge for the sample annealed at 600 °C. As expected, the (101) peaks gain intensity at the Zn edge and the (204) peaks lose intensity. The shoulder on the (204) peak at lower Q-value is the (220) peak which is located right next to the (204).

 This journal is © The Royal Society of Chemistry 2020

Published on 12 March 2020. Downloaded by Northwestern University on 9/29/2020 9:16:38 PM.

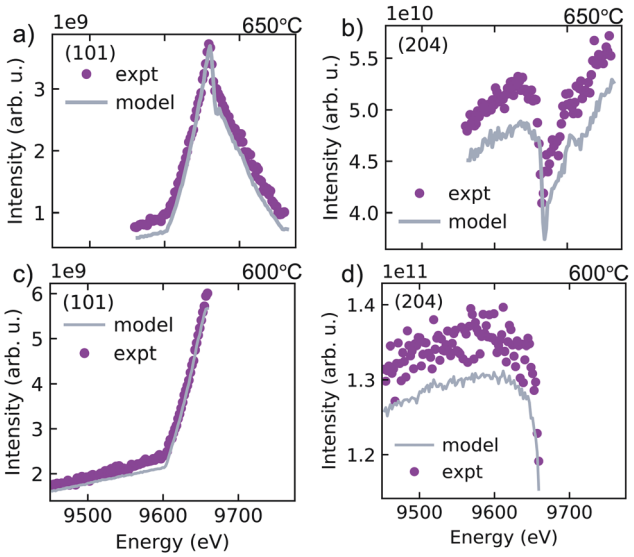

Fig. 4 Rietveld refinement results for the peak intensities as a function of X-ray energy for (a) the (101) and (b) (204) peaks measured on the sample annealed at 650 °C, and (c) the (101) and (d) the (204) peaks measured on the sample annealed at 600 °C. Due to artifacts in the detector image at energies above the Zn edge, only data up to the edge was used for the 600 °C sample.

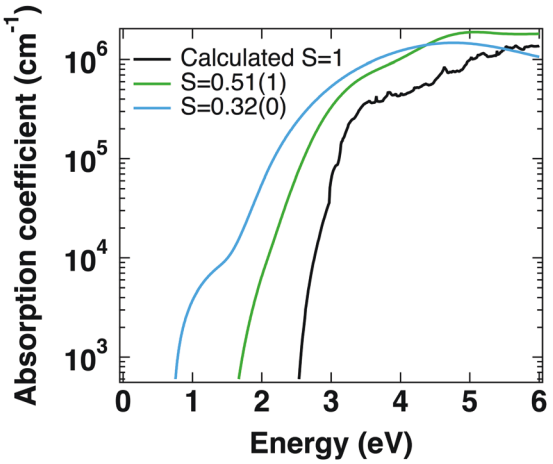

Fig. 5 Absorption coefficient curves for the two partially ordered samples and the calculated absorption for a fully ordered $ZnGeP_2$ structure. The two partially ordered samples have an absorption onset lower than that calculated for the fully ordered structure. The absorption coefficient for the fully ordered structure was obtained from GW calculations.[28]

was calculated using the cation site occupancies: $S = Zn_{Zn} + Ge_{Ge} - 1$, where Zn_{Zn} is the fraction of Zn on the Zn site and Ge_{Ge} is the fraction of Ge on the Ge site. The uncertainty in the order parameter was calculated using the uncertainty in the average site occupancies, determined in TOPAS based on the model fit. A slight offset in the intensity of the model compared to the experimental data can be seen in Fig. 4(b) and (d), however this offset is less than 10% so it would not change the calculated order parameter within the significant figures we are reporting. The calculated order parameter for the sample annealed at 650 °C with $\frac{c}{a}$ of 1.963(1) was 0.51(1). The order parameter determined for the sample annealed at 600 °C, with a $\frac{c}{a}$ of 1.968(3), was 0.32(0). This difference between the measured site occupancies and that expected from $\frac{c}{a}$ could indicate that the relationship between the two is not a simple linear relationship. One possible explanation is that for any given S there exists a range of corresponding $\frac{c}{a}$ values, or *vice versa*, and the kinetics involved in the growth process determine which S and $\frac{c}{a}$ are realized. However, further experimental and computational work needs to be done to shed light on this process. Additionally, our results could suggest that neither $\frac{c}{a}$ or S is sufficient on its own to fully explain ordering in a complex ternary system. Both metrics lack information on the short range order, which could have profound effects on properties.

The complexities in characterizing ordering and its effects have been illustrated in work on the effects of short and long range order in II–IV–N_2's. In $ZnSnN_2$ and $ZnGeN_2$, it has been predicted that local octet-rule-violating bonding environments have the greatest impact on optoelectronic properties. It was found that an increased concentration of octet rule violating motifs causes a narrowing of the band gap and less steep absorption onset, while octet rule preserving disorder has hardly any effects on electronic structure.[24–26] Our absorption coefficient results for the $ZnGeP_2$ films, shown in Fig. 5, show a lower energy absorption onset in the two films compared to the calculated absorption coefficient. The smaller band gap of partially disordered films is consistent with the predicted behavior for octet rule violating disorder, although additional measurements that directly probe short range order are needed to better confirm this hypothesis. However, our absorption results do suggest that S is better capturing the cation site disorder than $\frac{c}{a}$.

The discrepancy we have found between $\frac{c}{a}$ and S illustrate the difficulties in choosing a metric for quantifying cation disorder. While stretching parameters and long range order parameters have both been used in the literature to describe disorder, they are each probing different aspects of the material and as a result may not trend in identical ways with material properties, as we have seen with the absorption coefficient. This work highlights the importance of choosing a metric for disorder that most accurately reflects the physical properties of interest. In this work, it is clear that S is better representing the disorder that is causing changes in absorption, although further work is needed to determine if an analysis of the short range order could provide insight into the type of disorder that is present. However, if instead we were interested in anisotropic optical properties and birefringence, it is possible that $\frac{c}{a}$ would be the more important metric to analyze.

The absorption results also illustrate the strong potential for $ZnGeP_2$ in optoelectronic devices, in particular as a top cell material in Si tandem solar cells. These results also show the ability to tune the band gap of $ZnGeP_2$ using cation site disorder.

Published on 12 March 2020. Downloaded by Northwestern University on 9/29/2020 9:16:38 PM.

In our films we see lowering in the absorption onset with increased disorder to below 2 eV, close to the 1.7 eV ideal band gap for a top cell material on Si.[27]

4 Conclusions

We have conducted a study on two different methods for quantifying order in ternary semiconductors: $\frac{c}{a}$, a stretching parameter determined from lattice constants and S, a long range order parameter calculated from the average site occupancies. A discrepancy was found between the two metrics when it was determined that films with an "ordered" $\frac{c}{a}$ had only partially ordered cation site occupancies, resulting in an S of less than 1. Optical absorption results for the films showed a decrease in absorption onset energy, consistent with the effects of octet-rule-violating disorder in II–IV–N_2's, suggesting that some disorder was indeed present in the films.[24–26] From the absorption results it is clear that S is better capturing the disorder in these films and is a more useful metric of disorder if interested in optical absorption properties. This work highlights the subtle differences between various metrics for quantifying order and the importance in determining which metric will best represent changes in the material properties of interest.

Conflicts of interest

There are no conflicts to declare.

Acknowledgements

This work was authored in part by Alliance for Sustainable Energy, LLC, the manager and operator of the National Renewable Energy Laboratory for the U.S. Department of Energy (DOE) under Contract No. DE-AC36-08GO28308. Primary support for this work was provided by the U.S. Department of Energy, Office of Science, Basic Energy Sciences, Materials Sciences and Engineering Division. R. R. S. acknowledges support from the National Science Foundation Graduate Research Fellowship under Grant No. 1646713. B. L.-W. acknowledges support from the National Science Foundation Graduate Research Fellowship under Grant No. DGE-114747. B. L.-W., M. F. T., and E. S. T. acknowledge support from the National Science Foundation, DMREF No. 1729594. Use of the Stanford Synchrotron Radiation Lightsource, SLAC National Accelerator Laboratory, is supported by the DOE Office of Science (SC), Basic Energy Sciences (BES) under Contract No. DE-AC02-76SF00515. The authors are also grateful to Jacob Cordell and Dr Stephan Lany for many helpful discussions.

Notes and references

1 M. A. Green, *J. Mater. Sci.: Mater. Electron.*, 2007, **18**, 15–19.
2 A. D. Martinez, E. S. T. Angela, N. Fioretti and A. C. Tamboli, *J. Mater. Chem. A*, 2017, **5**, 11418–11435.
3 S. Hall, J. Szymanski and J. Stewart, *Can. Mineral.*, 1978, 131–137.
4 H. Nozaki, T. Fukano, S. Ohta, Y. Seno, H. Katagiri and K. Jimbo, *J. Alloys Compd.*, 2012, **524**, 22–25.
5 J. Paier, R. Asahi, A. Nagoya and G. Kresse, *Phys. Rev. B: Condens. Matter Mater. Phys.*, 2009, **79**, 115126.
6 S. Schorr, H.-J. Hoebler and M. Tovar, *Eur. J. Mineral.*, 2007, **19**, 65–73.
7 S. Siebrentritt and S. Schorr, *Prog. Photovolt.: Res. Appl.*, 2012, **20**, 512–519.
8 S. Chen, X. G. Gong, A. Walsh and S.-H. Wei, *Phys. Rev. B: Condens. Matter Mater. Phys.*, 2009, **79**, 165211.
9 S. Schorr, *Sol. Energy Mater. Sol. Cells*, 2011, **95**, 1482–1488.
10 S. Schorr, C. Stephan, T. Torndahl, R. Gunder and D. M. Tobbens, *X-ray and Neutron Diffraction on Materials for Thin-Film Solar Cells*, John Wiley Sons, Ltd, 2016, ch. 15, pp. 421–440.
11 B. Warren, *X-ray Diffraction*, Dover Publications, Mineola, NY, 1990.
12 S. Nakatsuka and Y. Nose, *J. Phys. Chem. C*, 2017, **121**, 1040–1046.
13 E. W. Blanton, K. He, J. Shan and K. Kash, *J. Cryst. Growth*, 2017, **461**, 38–45.
14 L. Garbato, F. Ledda and A. Rucci, *Prog. Cryst. Growth Charact. Mater.*, 1987, **15**, 1–41.
15 B. Ray, A. Payne and G. Burrell, *Phys. Status Solidi*, 1969, 197–204.
16 K. Masumoto, S. Isomura and W. Goto, *J. Phys. Chem. Solids*, 1966, **27**, 1939–1947.
17 K. H. Stone, S. T. Christensen, S. P. Harvey, G. Teeter, I. L. Repins and M. F. Toney, *Appl. Phys. Lett.*, 2016, **109**, 161901.
18 L. T. Schelhas, K. H. Stone, S. P. Harvey, D. Zakhidov, A. Salleo, G. Teeter, I. L. Repins and M. F. Toney, *Phys. Status Solidi B*, 2017, **254**, 1700156.
19 P. F. Ndione, Y. Shi, V. Stevanovic, S. Lany, A. Zakutayev, P. A. Parilla, J. D. Perkins, J. J. Berry, D. S. Ginley and M. F. Toney, *Adv. Funct. Mater.*, 2014, **24**, 610–618.
20 A. D. Martinez, E. M. Miller, A. G. Norman, R. R. Schnepf, N. Leick, C. Perkins, P. Stradins, E. S. Toberer and A. C. Tamboli, *J. Mater. Chem. C*, 2018, **6**, 2696–2703.
21 R. R. Schnepf, A. D. Martinez, J. S. Mangum, L. T. Schelhas, E. S. Toberer and A. C. Tamboli, *Proceedings of 46th IEEE PVSC*, 2019.
22 G. Kimmel, Y. Shimony, O. Raz and M. Dariel, *Mater. Struct.*, 1999, **6**, 149–151.
23 M. D. Lind and R. Grant, *J. Chem. Phys.*, 1973, **58**, 357–362.
24 P. C. Quayle, E. W. Blanton, A. Punya, G. T. Junno, K. He, L. Han, H. Zhao, J. Shan, W. R. L. Lambrecht and K. Kash, *Phys. Rev. B: Condens. Matter Mater. Phys.*, 2015, **91**, 205207.
25 D. Skachkov, P. C. Quayle, K. Kash and W. R. L. Lambrecht, *Phys. Rev. B*, 2016, **94**, 205201.
26 S. Lany, A. N. Fioretti, P. P. Zawadzki, L. T. Schelhas, E. S. Toberer, A. Zakutayev and A. C. Tamboli, *Phys. Rev. Mater.*, 2017, **1**, 035401.
27 T. J. Coutts, J. S. Ward, D. L. Young, K. A. Emery, T. A. Gessert and R. Noufi, *Prog. Photovolt.: Res. Appl.*, 2003, **11**, 359–375.
28 High Performance Computing Center Materials Database, materials.nrel.gov.

 This journal is © The Royal Society of Chemistry 2020